Journal of Applied Electrochemistry **34**: 751–756, 2004.
© 2004 *Kluwer Academic Publishers. Printed in the Netherlands.*

Uniform thin film electrodeposition onto large circular wafer substrates

HECTOR ORTIZ-IBARRA and J. ANTONIO MEDINA*
Departamento de Quimica, Universidad de Guadalajara, Calz. M. Garcia Barragan 1451 CP 44420 Guadalajara, Mexico
(**author for correspondence: Current address: Seagate Technology, 7801 Computer Avenue South, Bloomington, MN 55435, USA, e-mail: jose.a.medina@seagate.com*)

Received 27 January 2003; accepted in revised from 2 February 2004

Key words: paddle cell, uniform current distribution, uniform injection cell, wafer electroplating

Abstract

A wafer-scale electrochemical flow cell specially suited for uniform thin-film electrodeposition is presented. The cell consists of a porous disk injector set parallel and coaxial to a working disk electrode with a narrow separation gap between them. The porous injector was designed to supply a uniform axial flow of electrolyte onto the surface of the working disk electrode. The mass transfer characteristics of the cell and the current distribution on the working disk electrode were studied for various operating conditions, geometric parameters and bath chemistries. The experimental results confirmed the simple scaling properties that were theoretically predicted. It has also been shown that this cell can provide nearly uniform current distribution on the working electrode under conditions of both migration and convective-diffusive mass transfer control. The results indicate that this cell is suitable for uniform thin-film electrodeposition onto large circular wafer substrates.

1. Introduction

Modern magnetic and electronic device fabrication processes require sophisticated patterning, deposition and etching techniques to produce structures with well-defined sub-micron features [1]. The increasing complexity of modern device manufacturing processes has led to cost-saving strategies that include the use of larger wafer substrates for higher-volume production. Manufacturers of magnetic recording heads, for instance, have adopted larger circular wafers substrates (diameter $\geqslant 6''$) in the last few years, thus lowering the production costs as the areal-density recording nearly doubles every year [2, 3].

When migrating to larger wafer substrates, the high-yield and performance of the fabrication processes may be compromised if the processing equipment is not adequately re-scaled. Equipment re-scaling is generally difficult when the fundamental principles of the process and the scale-up characteristics of the system are not well understood [4].

Consider for instance the case of thin-film electrodeposition in reciprocating paddle cells. Paddle cells have been successfully used in device manufacturing processes for nearly three decades [5]. However, scaling a paddle cell to accommodate larger wafer substrates is frequently limited to simple modification of the plating fixture to fit the new wafer size. In many cases, no effort is made to redesign the geometry and the dimensions of the cell compartment, the anode, the current thief, and the paddle. Moreover, guidelines are rarely available for setting new cell parameters such as paddle speed, ratio of wafer to thief current and flow of electrolyte. This may be due to the fact that only semi-empirical models for convective-diffusive mass transport can be derived for this cell configuration owing to its complicated hydrodynamic characteristics [6]. Additionally, it is a difficult task to predict the current distribution on the wafer substrate and its dependence on the plating parameters, the system geometry and the electrolyte properties [7]. These complications may result in plated films with uniformities that are currently unacceptable in device microfabrication processes.

An electrochemical cell that provides spatially-uniform convective mass transport and uniform primary current distribution on the plating substrate, and at the same time is easy to scale-up, is very desirable in device fabrication processes [4]. However, commercially available electrochemical cells typically possess some, but not all, of these desirable features [8].

An electrochemical flow cell referred to as the uniform injection cell (UIC) was introduced in recent years as a viable alternative that combines the above desirable features for device fabrication [4]. The UIC design consists of a working disk electrode (WE) of radius R and a porous disk injector of the same size that are placed parallel and coaxial to each other with a small gap L in between (see Figure 1). The electrolyte in the UIC is injected uniformly through the porous injector into the gap region. It has been theoretically predicted that the UIC can provide uniform mass-transfer-limited

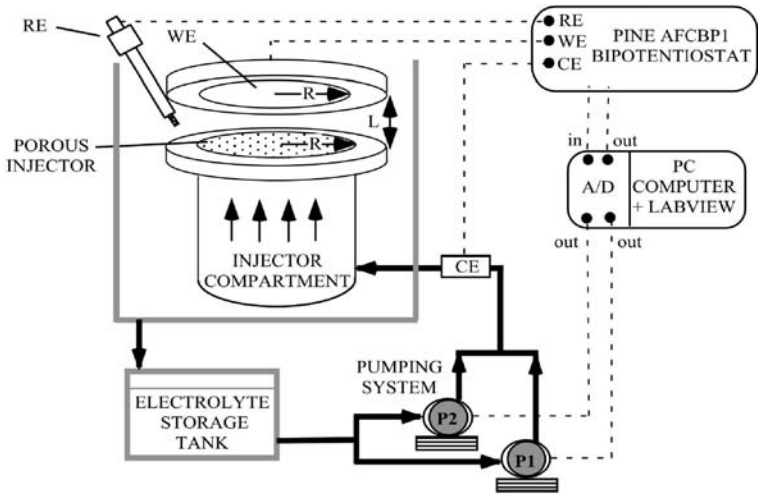

Fig. 1. Simplified diagram of the wafer-scale uniform injection cell (UIC).

current density and nearly uniform primary current distribution across the working electrode [8]. These unique features, hard to find in commercially available electrochemical cells, suggest that the UIC is suitable for uniform thin film electrodeposition under practically any operating condition.

Preliminary experimental work on the characterization of steady-state and flow-modulated convective mass transport in laboratory-scale versions of the UIC corroborated some of the theoretical predictions [9–11]. Intrinsic limitations, however, prevented the use of high flow rates of electrolyte. Additionally, narrow gap lengths between the working electrode and the electrolyte injector were hard to set and issues of non-uniform flow of electrolyte through the porous injector were present. It was predicted that scale-up versions of the UIC would overcome these and other limitations [9].

In this work we designed and characterized a wafer-scale version of the UIC. Results on convective mass transport, current distribution and alloy plating capability of the cell are presented.

2. Experimental

2.1. *Electrochemical cell*

A simplified diagram of the wafer-scale uniform injection cell is presented in Figure 1. The cell consisted of a 3″-diameter working disk electrode (WE) fabricated from corrosion resistant stainless steel. After mirror finishing one of its surfaces, the working electrode was sputter-deposited with 3000 Å of gold seed layer. Then, it was positioned at the center of a 5″-diameter circular Teflon holder maintaining its surface flush with the holder surface.

The injector compartment consisted of a cylindrical vessel with inner diameter of 3″, outer diameter of 5″, and height of 6.5″ made of a copolymer of polyester resin and styrene. This construction material was chosen due to its excellent mechanical strength and resistance to aggressive chemical environments. The porous injector included more than 1500 perforations with diameter of 1 mm and length of 2 cm that were individually drilled on the upper flat surface of the injector compartment. To enhance the spatial uniformity of the electrolyte flow, the perforations were uniformly distributed onto the injector surface using a hexagonal pattern and provided an open surface area of approximately 25%. Additionally, the injector compartment was packed with glass spheres of 22 mm in diameter to improve the flow uniformity across the injector surface.

The working disk electrode and the porous injector in the cell were set parallel and coaxial to each other with a narrow gap L between them (see Figure 1). An x–y–z positioner was used to set the gap L with an accuracy of ± 0.1 mm. Gap lengths of $L \leqslant 7.5$ mm allowed to maintain the aspect ratio L/2R under 0.1 that is recommended for improved current uniformity on the wafer surface for this cell configuration [8].

For the characterization of mass transport, a gold wire with a diameter of 1 mm and length of 2 m was used as a counter electrode (CE). The counter electrode was placed within the inlet tube of the injector compartment. For NiFe and for Cu electroplating, the counter electrode consisted of a nickel wire and of a copper foil respectively.

A venting tube helped remove gas bubbles from the electrolyte before it entered the injector compartment. A saturated calomel reference electrode (RE) was positioned with its tip within the gap region between the disk electrode and the porous injector (see Figure 1).

The pumping system consisted of standard PVC tubing, connectors, valves, and two corrosion resistant centrifugal pumps (P1 and P2 in Figure 1) with nominal power of 1/40 HP and 1/20 HP respectively. The pumps were coupled in parallel with a common discharge connected to the injector compartment. The pumping system was capable of delivering continuous or alternated flow of electrolyte of up to 14 $dm^3\ min^{-1}$. The

electrolyte storage tank had a maximum capacity of 15 dm^3. The operation of the pumping system was automated with an ATMIO16XE-50 A/D board from National Instruments and custom programs written in the LabView software package from the same company. Electrochemical experiments were performed with a Pine AFCBP1 bipotentiostat whose operation was automated and synchronized with the operation of the pumping system via the A/D board.

2.2. *Characterization of convective mass transport and current distribution*

The average flow rate in the experimental cell was calibrated with de-ionized water and it was determined that it was not affected by L values as low as 1 mm. The flow distribution across the injector surface was visually monitored using a black tracer that was delivered through the inlet tube of the injector compartment. These measurements confirmed that packaging glass spheres in the injector compartment may significantly improve the flow distribution across the injector surface. The flow uniformity was indirectly probed by comparing experimental results for steady-state convective-diffusive mass transport with theoretical predictions for this cell configuration [8].

The reduction of Fe(III) to Fe(II) was used to characterize steady and unsteady convective mass transport in the electrochemical cell. For this purpose, a well-supported electrolyte consisting of 5 mM Fe(II)/Fe(III) (prepared from sulfate salts) and 1 M H_2SO_4 (T=24 °C) was used in all the limiting-current experiments. For steady-state mass transfer characterization, constant injection flows in the range of 0–14 $dm^3\ min^{-1}$ and gap lengths (L) in the range of 1–5 mm were employed. In these experiments, the working disk electrode was maintained at a constant potential of −0.22 V vs a saturated calomel electrode (SCE) which was well within the mass transfer limited region for the redox couple and the conditions used in this work.

For unsteady convective mass transfer characterization, the flow of electrolyte was periodically modulated between 2.8 and 14 $dm^3\ min^{-1}$ at frequencies in the range of 0.025–1.5 Hz. The flow of electrolyte was modulated by alternating the operation of the centrifugal pumps (P1 and P2 in Figure 1) via the A/D board.

The current distribution was indirectly determined from the radial thickness profiles of electrodeposited copper films under the assumption that the current efficiency was uniform across the wafer during the plating process. On the other hand, discrete radial thickness profiles of the plated films were evaluated from the anodic stripping charge of nine distinct concentric circular regions on the wafer surface using Faraday's law.

2.3. *Flow-induced composition modulated NiFe alloys*

Flow-induced composition-modulated NiFe alloys (NiFe CMAs) were electroplated galvanostatically in the UIC and then they were stripped potentiostatically in the way described in Ref. [12] in order to analyze their structure. The electroplating bath in these experiments had a composition that was optimized for the electrodeposition of flow-induced NiFe CMAs [13]. The plating solution consisted of 0.2 M nickel sulfamate, 0.01 M iron chloride, 0.4 M boric acid, 1 g dm^{-3} ascorbic acid, 1.5 g dm^{-3} sodium saccharin, and 0.2 g dm^{-3} sodium dodecyl sulfate. The stripping solution, on the other hand, consisted of 0.2 M HCl and 0.5 M NaCl. The stripping experiments were carried out at a constant potential of 0.3 V vs SCE. In order to increase the plating and the stripping current densities in these experiments, the plating area of the working disk electrode was reduced to 16.3 cm^2 by covering part of its surface with a thin layer of a polymeric material.

3. Results and discussions

3.1. *Steady-state convective mass transport*

Steady-state convective mass transport in the wafer-scale UIC is appropriately characterized in terms of the Sherwood number (Sh) dependence on the Reynolds (Re) and Schmidt (Sc) numbers. The Sherwood number is defined by

$$Sh = \frac{KL}{D_i} = \frac{j_l}{nFC_i}\frac{L}{D_i} \tag{1}$$

where L is the gap length, n the number of electrons transferred, F is Faraday number, D_i the diffusion coefficient of the dilute reactant (i), K the mass transfer coefficient and C_i the concentration of i at the injector surface. The Reynolds and the Schmidt numbers are defined as $Re=VL/\upsilon$ and $Sc=\upsilon/D_i$, respectively, where V is the injection velocity and υ the kinematic viscosity of the electrolyte. Using the leading-order terms of perturbation series expansions for Sh, simple relationships have been derived for viscosity-dominated flow (Re«1)

$$Sh = 1.12\ Re^{1/3}Sc^{1/3} \tag{2}$$

and for convection-dominated flow (Re»1) in the UIC [8].

$$Sh = 0.85\ Re^{1/2}Sc^{1/3} \tag{3}$$

Therefore, a plot of $Sh/Sc^{1/3}$ vs Re provides a universal representation of steady-state convective mass transport in the UIC. A change in slope from 1/3 to 1/2 indicates transition between laminar and turbulent flow regimes [8]. Figure 2 presents experimental and theoretical steady-state convective mass transfer results (symbols and continuous line respectively) for the UIC as a plot of $Sh/Sc^{1/3}$ vs Re. The results for the reduction of Fe^{+3} to Fe^{+2} are in good general agreement with the theoretical predictions [8] in the range $1 \leqslant Re \leqslant 300$.

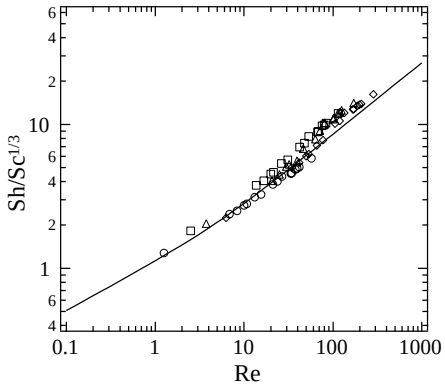

Fig. 2. Comparison between experiments (symbols) and theoretical results (continuous line) for mass transport in the wafer-scale UIC in terms of $Sh/Sc^{1/3}$ vs *Re*. Gap lengths of (○) 1 mm, (□) 2 mm, (△) 3 mm, and (◇) 5 mm.

Additionally, these results confirm the simple scale-up characteristics of the uniform injection cell and provide indirect evidence of good flow uniformity across the surface of the porous injector.

3.2. *Flow-modulated convective mass transport*

The limiting current response to flow oscillations was used to determine the non-steady convective mass transport characteristics of the UIC. With these experiments we also determined the ability of the pumping system to execute predetermined flow modulation programs. It has been demonstrated that appropriate flow manipulation can be used in the electrodeposition of complicated laminated structures from single electrolytes [10–15]. The UIC, unlike paddle cells and other common cell configurations, offers the possibility to create flow-induced laminated structures in device manufacturing processes [15].

To determine the frequency dependence of modulated limiting current in the UIC, the injection velocity was oscillated using square waveforms with frequencies in the range of 0.025–1.5 Hz. We found that a quasi-steady limiting current response (modulation period » mass transfer relaxation time) can be obtained for modulation frequencies as high as 0.25 Hz. However, significant attenuation of the modulated limiting current response was observed for modulation frequencies greater than approximately 0.5 Hz. Theoretical studies on the dynamics of limiting current in a flow-modulated UIC subjected to large sinusoidal modulations indicate that a quasi-steady response can be obtained for modulation frequencies in the above range [16]. Well-controlled quasi-steady flows are generally adequate for the electrodeposition of complex laminated structures from single electroplating baths [12, 15].

Figure 3 shows a typical quasi-steady limiting current response to flow modulation. In this case, the flow of electrolyte was modulated between 2.8 and 14 $dm^3\ min^{-1}$ at a frequency of 0.025 Hz using a square waveform (part A). The limiting current response (part B) corresponds to the reduction of Fe^{+3} to Fe^{+2} for $L = 2$ mm. A quasi-steady response is indicated by a nearly-square limiting current waveform where the maximum and minimum values correspond to the steady-state values for the maximum and minimum flow rates, respectively.

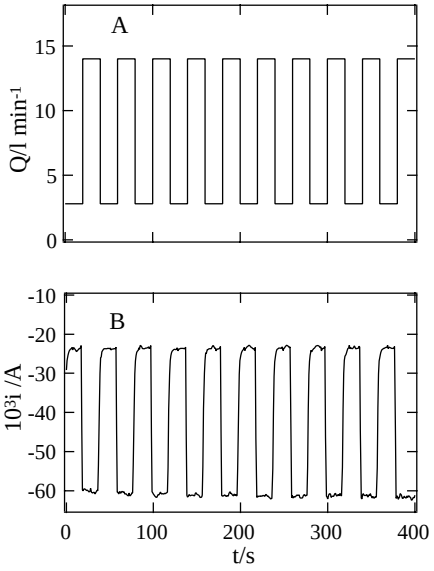

Fig. 3. Limiting current response for the reduction of Fe(III) to Fe(II) in the UIC using an oscillating flow of electrolyte. (A) Flow modulation as a function of time with minimum and maximum flows of 2.8 and 14 $dm^3\ min^{-1}$ respectively and modulation frequency of 0.025 Hz. (B) Limiting current response as a function of time.

3.3. *Electrodeposition of composition-modulated nickel–iron alloys*

Experiments on galvanostatic deposition of NiFe alloys were carried out in the wafer-scale UIC using an oscillating flow of electrolyte. Then, the electroplated films were potentiostatically stripped in the same cell after the plating solution was replaced by a well-supported electrolyte containing ionic species that were not electroactive at the stripping potential. Periodic oscillations in the stripping curve indirectly confirm the presence of a compositionally modulated structure [12, 15].

Figure 4 presents a potentiostatic stripping curve of a NiFe film that was electroplated in the wafer-scale UIC using the plating solution described in the experimental section at a constant current density of $-25\ mA\ cm^{-2}$ and a plating time of 500 s with $L = 1$ mm. The electrolyte flow was modulated using a square waveform with a maximum flow of 13.1 $dm^3\ min^{-1}$, a minimum flow of 1 $dm^3\ min^{-1}$ and a modulation frequency of 0.01 Hz. Thereafter, the plated film was stripped in the UIC using the stripping solution described in the experimental section, a constant potential of 0.3 V vs SCE and a constant flow of 5 $dm^3\ min^{-1}$. The oscillations in the stripping curve in Figure 4 show the presence of a composition-modulated NiFe structure,

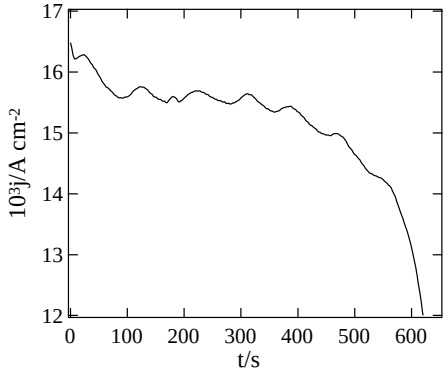

Fig. 4. Potentiostatic stripping curve for a NiFe film that was electroplated in the UIC using an oscillating flow of plating electrolyte. The film was stripped in the UIC at a constant oxidation potential of 0.3 V vs SCE and constant flow rate of 5 dm^3 min^{-1}. The stripping solution consisted of 0.2 M HCl and 0.5 M NaCl.

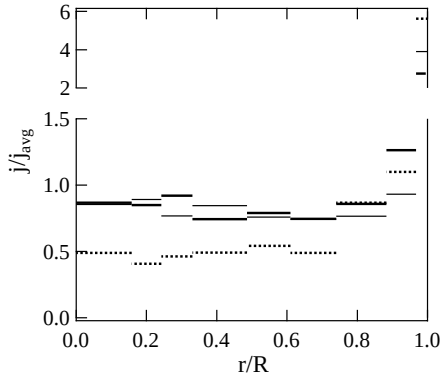

Fig. 5. Radial current density distribution on the working disk electrode of the wafer-scale UIC for $L = 1$ mm (thin continuous lines), $L = 4$ mm (thick continuous lines), and for no injector compartment in place (dashed lines). The profiles were indirectly evaluated from thickness measurements of electroplated copper films. The current density and the radial position are normalized with respect to the average current density and to the radius of the working disk electrode respectively.

since the oxidation kinetics for NiFe significantly depends on the iron content. In this case, faster oxidation kinetics corresponds to iron-enriched NiFe materials [12, 15]. Qualitatively, these experiments show that well-controlled quasi-steady flow in the UIC can be used to fabricate laminated plated structures in systems where one or more species deposit under mass transfer control.

The more attenuated modulations on the stripping curves (see Figure 4), compared to those of flow-modulated rotating disk electrodes [10, 12, 14], indicate that our stripping conditions were not optimal. Namely, the stripping potential was selected so that the stripping current did not exceed the nominal output of our potentiostat (1 A). Higher stripping current may result in a better defined stripping waveform which in combination with an *in situ* technique for Ni or Fe detection would allow us to depth profile the laminated structure. Consider for instance that a concentric ring electrode can be used during the stripping process to oxidize Fe^{+2} released from the disk electrode into Fe^{+3} in order to determine the composition depth profile and the wave length of laminated NiFe films [12, 17].

3.4. *Current distribution*

The current distribution on the working disk electrode was indirectly determined from the stripping charge of electroplated copper films as described in the experimental section. Although our discrete stripping procedure did not produce rigorous quantitative information on the film thickness profiles, it proved to be a valuable and inexpensive alternative when thickness profiling equipment is not readily available. The purpose of these experiments was to determine the current distribution on the working disk electrode under the worst case conditions where ion migration is the dominant transport mechanism. Under these conditions, near primary current distribution is expected on the working disk electrode [7]. An unsupported diluted electrolyte consisting of 17 g dm^{-3} $CuSO_4$ was used to electrodeposit copper films with average thickness of approximately 2 μm. A current density of -4.1 mA cm^{-2}, plating time of 33 min, and flow rate of 5.7 dm^3 min^{-1} were used in the electroplating experiments. The low electrolyte conductivity and plating current density well under the mass transfer limiting value provided conditions for migration-dominated transport in the system.

Figure 5 presents the radial current density distribution on the working disk electrode of the wafer-scale UIC evaluated from the copper plating experiments described above. The horizontal lines in this figure show the average current density for each annular section on the working electrode surface. In this figure, the current density and the radial position were normalized with respect to the average current density and to the radius of the working disk electrode, respectively. The thin and the thick continuous lines in Figure 5 correspond to copper plating experiments in the UIC using gaps of $L = 1$ and 4 mm, respectively. The dashed lines in Figure 5 correspond to the case where the injector compartment (shown in Figure 1) was removed during the plating process (e.g. $L \to \infty$). These experimental results show that a narrower gap L in the UIC can lead to a more uniform current distribution on the working disk electrode. Moreover, the role played by the porous injector in improving the current uniformity is demonstrated. These experimental results identify the following regions of uniform current distribution on the working disk electrode: $r/R < 0.96$ for $L = 1$ mm, $r/R < 0.9$ for $L = 4$ mm, and $r/R < 0.75$ for $L \to \infty$.

Although the thickness of the electroplated copper films on which the current distribution calculations were based could not be measured in a more direct and accurate way, the qualitative trends shown in Figure 5 have been theoretically predicted for the UIC. Figure 6 presents theoretical results for the primary current

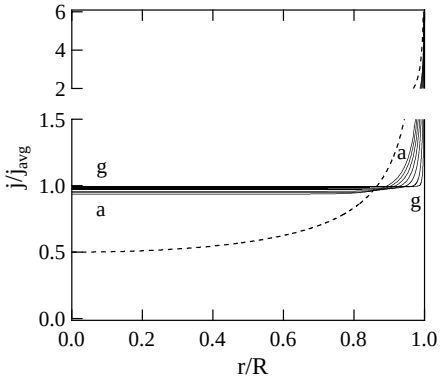

Fig. 6. Primary current distribution on the working disk electrode of the UIC [8]. The continuous curves correspond to gap aspect ratios $L/2R$ = (a) 0.15, (b) 0.125, (c) 0.1, (d) 0.075, (e) 0.05, (f) 0.025, and (g) 0.01. Only curves (a) and (g) are labeled on the plot. The dashed line corresponds to the primary current distribution for a disk electrode with a distant counter electrode.

distribution in the UIC [8]. The continuous curves correspond to gap aspect ratios $L/2R$ from 0.15 (curve a) to 0.01 (curve g). The dashed line corresponds to the theoretical primary current distribution for a disk electrode with a distant counter electrode. A Remarkable resemblance is observed between the experimental results in Figure 5 and the theoretical results in Figure 6 for primary current distribution in the UIC. These results suggest that migration is the dominating transport mechanism for the copper plating experiments described above. Thus, it is shown that the uniform injection cell is capable of providing nearly uniform current distribution under the most adverse circumstances.

4. Conclusions

The rigorous requirements on the thickness uniformity of electroplated features with sub-micron dimensions in modern microfabrication applications are harder to achieve in conventional plating paddle cells. This is especially true for thin film electrodeposition onto large circular wafer substrates (diameter $\geqslant 6''$). Within-wafer standard deviation of 1% with respect to the mean, or better, is not an uncommon requirement for plated thickness uniformity in order to maintain satisfactory yields in applications such as magnetic recording heads. Achievable standard deviation of about 2% in standard paddle cells would result in lower than about 85% yield in order to satisfy the above uniformity requirement, significantly compromising the viability of the manufacturing process.

Since primary current distribution is the main contribution to the film thickness uniformity in the uniform injection cell, simple calculations indicate that a 1% standard deviation can be readily achieved in this cell under normal operating conditions [8]. Considering for instance an edge exclusion zone of 5% of the wafer radius, an aspect ratio of $L/2R \leqslant 0.066$ in this cell would result in thickness distribution with better than 1% standard deviation. For a $6''$ wafer diameter this requires an easy-to-set 1-cm gap between the wafer and the porous injector.

In this work we have demonstrated that the uniform injection cell is easy to scale and that improved thickness uniformity can be achieved without the need for current thieves, divided anodes or moving parts. Thus, this cell design is worth considering for high-yield electrodeposition onto large circular wafer substrates.

Acknowledgements

We acknowledge the Mexican National Concil for Science and Technology (CONACyT) for support of this research (Project No. I28149U). H. Ortiz-Ibarra thanks CONACyT for support through a Graduate Fellowship.

References

1. M. Madou, '*Fundamentals of microfabrication*' (CRC Press, Boca Raton, New York, 1997).
2. J. Best and V. Marrello, *in* S. Krongelb, W. Schwarzacher, L.T. Romankiw, C.H. Ahn and J.-W. Chang (Eds), Proceedings of the VI International Symposium on Magnetic Materials Processes and Devices, PV 2000-29 (The Electrochemical Society, Pennington, NJ, 2000), p. 3.
3. J.N. Porter, *in* S. Krongelb, W. Schwarzacher, L.T. Romankiw, C.H. Ahn and J.-W. Chang (Eds), Proceedings of the VI International Symposium on Magnetic Materials Processes and Devices, PV 2000-29, (The Electrochemical Society, Pennington, NJ, 2000), p. 19.
4. J.A. Medina, D.L. Sexton, and D.T. Schwartz, *in* M. Datta, K. Sheppard and J. Dukovic (Eds), Proceedings of the II International Symposium on Electrochemical Microfabrication, PV 94-32, (The Electrochemical Society, Pennington, NJ, 1995), p. 154.
5. J.V. Powers and L.T. Romankiw, U.S. Pat. 3,652,442 (1972).
6. D.T. Schwartz, B.G. Higgins, P. Stroeve and D. Borowski, *J. Electrochem. Soc.* **134** (1987) 1639.
7. J.S. Newman, '*Electrochemical systems*' (Prentice-Hall, Englewood Cliffs, NJ, 1973), p. 344.
8. J.A. Medina and D.T. Schwartz, *J. Electrochem. Soc.* **142** (1995) 451.
9. J.A. Medina, D.L. Sexton and D.T. Schwartz, *J. Electrochem. Soc.* **142** (1995) 457.
10. S.D. Leith and D.T. Schwartz, *Electrochim. Acta* **44** (1999) 4017.
11. S.D. Leith and D.T. Schwartz, *J. Microelectromech. Syst.* **9** (1999) 384.
12. S.D. Leith, S. Ramli and D.T. Schwartz, *J. Electrochem. Soc.* **146** (1999) 1431.
13. S.D. Leith and D.T. Schwartz, *J. Electrochem. Soc.* **143** (1996) 873.
14. S.D. Leith, W. Wang and D.T. Schwartz, *J. Electrochem. Soc.* **145** (1998) 2827.
15. J.A. Medina and D.T. Schwartz, *Electrochim. Acta* **42** (1997) 2679.
16. J.A. Medina and D.T. Schwartz, *J. Electrochem. Soc.* **144** (1997) 155.
17. P.C. Andricacos, J. Tabib, and L.T. Romankiw, *J. Electrochem. Soc.* **135** (1988) 1172.